ACS APPLIED NANO MATERIALS

www.acsanm.org

Article

In Situ P-Modified Hybrid Silica–Epoxy Nanocomposites via a Green Hydrolytic Sol–Gel Route for Flame-Retardant Applications

Aurelio Bifulco,* Roberto Avolio, Sandro Lehner, Maria Emanuela Errico, Nigel J. Clayden, Robin Pauer, Sabyasachi Gaan, Giulio Malucelli, Antonio Aronne, and Claudio Imparato*

Cite This: *ACS Appl. Nano Mater.* 2023, 6, 7422–7435

Read Online

ACCESS | Metrics & More | Article Recommendations | Supporting Information

ABSTRACT: Flame retardance of epoxy resins is usually imparted using suitable additives and/or properly modified curing agents. Herein, via a two-step green synthetic procedure, the chemical modification of the epoxy matrix with reactive silicon and phosphorus precursors is explored to obtain nanocomposites with intrinsic flame-retardant features. Nanoscale phase separation occurs in the first step, forming an inverse micelle system in which polar nanodomains act as nanoreactors for the hydrolysis of silanes (Si precursors), giving rise to silica lamellar nanocrystals (SLNCs). In the second step, inside the silica nanodomains, the formation of stable Si–O–P bonds occurs because the reactivity of phosphoric acid (P precursor) with the oxirane rings of the polymer chain is balanced by its tendency to diffuse into polar nanodomains. Intriguingly, the use of phosphoric acid alone in epoxy composite manufacturing leads to a wormlike morphology of the network, whereas its addition in the presence of silanes results in the formation of SLNCs with a thinner interlayer distance. The morphology of the hybrid Si/P–epoxy nanocomposites, comprising organic and inorganic co-continuous phases, can confer, through a prevalent mechanism in the condensed phase, interesting flame-retardant performances, namely, the absence of dripping during vertical burning tests, the formation of a large amount of coherent char after combustion, and a remarkable reduction (up to 27.7%) in the peak of heat release rate. The above characteristics make these nanostructured hybrid materials very promising for the manufacturing of epoxy systems with enhanced fire behavior (e.g., coatings, sealants, matrices for reinforced composites), even containing a low amount of specific flame retardants and thus keeping good viscoelastic properties.

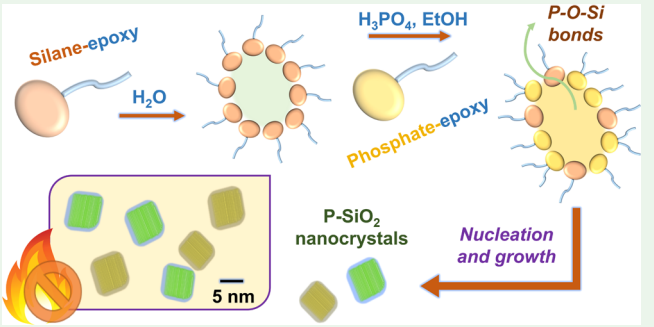

KEYWORDS: *sol–gel synthesis, hybrid nanocomposites, epoxy resin, silica nanodomains, phosphorus–silicon interactions, thermal behavior, flame retardance*

1. INTRODUCTION

Epoxy resins are widely used in several applications in the field of casting, composites, laminates, and electronic components because of their excellent properties, such as high chemical resistance and adhesion.[1,2] The low fire resistance of these materials, including the generation of toxic smoke and flammable gases during combustion, is the most serious restriction for their widespread application.[3−5] The usual approaches to enhance the flame retardance of epoxy resins include the addition of reactive or nonreactive flame retardants, the modification of the polymer matrix with suitable elements, mainly phosphorus and silicon, and the use of specific curing agents.[6]

The depletion of natural sources (including phosphorus) and the overuse of flame retardants (FRs) are two of the main challenges that have to be faced.[7,8] The in situ generation of hybrid organic–inorganic phases in epoxy composites is considered a valuable strategy to improve the fire behavior of epoxy resins, especially combined with P-based flame retardants (FRs). This approach, based on sol–gel chemistry, can result in an even distribution of inorganic nanostructures anchored throughout the polymer matrix. Thus it allows for avoiding the use of halogen-containing additives, which generate corrosive and toxic combustion products,[9,10] and preventing dripping phenomena, even using hardeners with high flammability (i.e., aliphatic compounds) and low loadings of P and inorganic fillers (e.g., silica, clay, or metal hydroxide particles).[11−14] Consequently, the use of low quantities of inorganic fillers facilitates the preservation of the mechanical performance of the nanocomposite. To obtain such features for aliphatic epoxy systems without any in situ sol–gel

Received: February 8, 2023
Accepted: April 14, 2023
Published: April 26, 2023

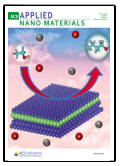

Scheme 1. Synthesis Procedure of Si/P−Epoxy Hybrid Nanocomposites and Simplified Representation of Their Possible Chemical Structures, Focusing on the Epoxy Chains Linked to the Inorganic Nanodomains[a]

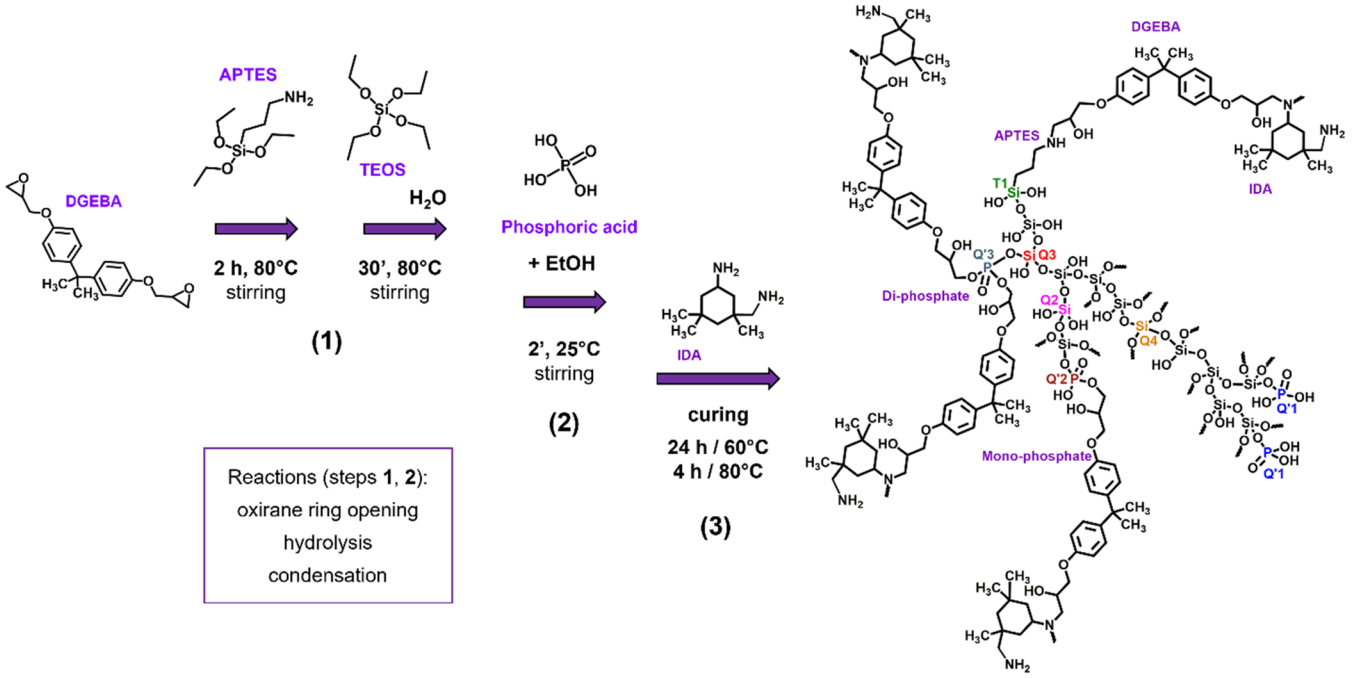

[a]Step 1: from the reaction of DGEBA with APTES, followed by the addition of TEOS and hydrolysis at 80 °C, epoxy−silica hybrid chains are obtained; step 2: the mixture is cooled to room temperature, and an ethanol solution of H_3PO_4 is added, giving fast reaction with DGEBA and/or silanes; step 3: the system is cured with IDA, a cycloaliphatic amine. In the illustrated structure, some T_N and Q_N units of Si and Q'_N units of P are indicated; this notation is explained in the text (Section 2.1).

modification, huge amounts of P (from 4 to 6 wt %) and inorganic fillers (∼15 wt %) together with a strong N−P synergism are usually required.[15−18] On the contrary, the use of ammonium polyphosphate (APP) or 9,10-dihydro-9-oxo-10-phosphaphenanthrene-10-oxide (DOPO) derivatives in combination with the generation of in situ sol−gel silica nanoparticles in an epoxy matrix led to self-extinguishing nanocomposites (V-0 rating in UL94 burning tests) with low P loadings (e.g., 1, 2 wt %), even using isophorone diamine (IDA) as a cycloaliphatic amine hardener.[19,20] However, it should be underlined that a high weight percentage of phosphorus-based FR is required to reach such P loadings.

The incorporation of P in an epoxy−silica network may be a promising strategy to reduce the flammability of aliphatic systems, preventing the need for a massive amount of FR additives. The effects of silica-based particles formed into epoxy resins on their thermal and mechanical properties have been extensively studied.[11,13,14,21] The presence of Si−O−P bonds in the hybrid polymer may lead to such interesting advantages as the uniform distribution of phosphorus, and the formation of Si- and P-containing structures in the char, resulting in enhanced stability and fire performance.[22−24] On the other hand, clear evidence for Si−O−P bonds in a polymeric matrix has never been reported until now, even if, in some works, their presence was hypothesized. Chiang and Ma[25] observed the presence of Si−O-Si and Si−O-C bonds in a hybrid system obtained by treating a bisphenol A diglycidyl ether (DGEBA) resin with tetraethyl orthosilicate (TEOS), a coupling agent (3-isocyanatopropyltriethoxysilane) and diethylphosphatoethyltriethoxysilane (DPTES), using THF as a solvent in the hydrolytic process; the resin was cured with 4,4′-diaminodiphenylsulfone. This hybrid organic−inorganic material showed an increase of residual char up to 16.2%, and the limiting oxygen index (LOI) was raised from 24 to 32% with respect to the polymer counterpart. Recently, Parida et al.[26] obtained hybrid silica nanoparticles using *N*,*N*′-bis[4,6-bis-(diethylphosphono)-1,3,5-triazin-yl]-1,2-diaminoethane as a P precursor and observed the occurrence of a strong structural rearrangement of Si units because of the presence of P. Overall, the in situ growth of Si−P mixed oxide nanostructures into epoxy resins and the potential role of such phases in determining the properties and behavior of the composites appear still largely unexplored.

In this work, a sustainable synthesis strategy is established to incorporate phosphorus into a hybrid epoxy−silica network without any use of aromatic precursors and hardeners or toxic reagents and solvents, employing only ethanol and water and phosphoric acid as a "green" P precursor. Starting from a route recently proposed, which allowed obtaining epoxy-based nanocomposites containing nanodomains of lamellar SiO_2 nanocrystals with a multi-sheet morphology,[12,27−29] a new structural modification based on a hydrolytic sol−gel process is proposed to include phosphorus into silica nanodomains, obtaining a stable network containing Si−O−P bonds, which is expected to enhance the fire and thermal performances of the nanocomposites. It should be underlined that it is a huge challenge to fulfill this goal for three main reasons: (a) the difficulty in controlling the phosphoric acid reactivity in the shortage of an organic solvent; (b) the intrinsic instability of Si−O−P bonds in an aqueous environment;[30−32] (c) the triple role (reagent, catalyst, and hardener) played by H_3PO_4. In the two-step synthetic route presented herein, a hybrid epoxy−silica matrix is first obtained by the reaction of a mixture of DGEBA, (3-aminopropyl)triethoxysilane (APTES), and TEOS

https://doi.org/10.1021/acsanm.3c00590
ACS Appl. Nano Mater. 2023, 6, 7422−7435

at 80 °C, and then is mixed with a H_3PO_4 solution at room temperature and subsequently cured with an aliphatic hardener (IDA). Following this strategy, different nanodomains formed by lamellar silica nanocrystals (grown without surfactant templates) and P-containing moieties are uniformly dispersed in the epoxy matrix allowing for the obtainment of a co-continuous organic−inorganic network. The intrinsic flame-retardant properties provided by this hybrid nanostructure open a variety of possible applications in fire-resistant epoxy-based composites to be used as circuit board substrates (e.g., for 5G network) and coatings, among others.

Solid-state NMR, HRTEM, SEM-EDX, and ATR-IR were exploited to investigate the structural features, morphology, and chemical composition of the hybrid epoxy nanocomposites. The thermal behavior was studied by thermogravimetric (TG) analysis, differential scanning calorimetry (DSC), and dynamic mechanical analysis (DMA). Pyrolysis-combustion flow calorimetry (PCFC), cone calorimetry, and UL94 vertical flame spread tests were carried out to assess the fire performances of the obtained nanocomposites.

2. RESULTS AND DISCUSSION

2.1. Synthesis, Structural, and Morphological Characterization. The synthesis of hybrid nanocomposites formed by an inorganic silica phase dispersed in the epoxy matrix has been studied widely.[33,34] Two main strategies were explored: (i) the addition of preformed silica nanoparticles to the epoxy resin as fillers[16,35] and (ii) the in situ growth of silica nanoparticles obtained by the hydrolytic polycondensation of suitable Si precursors added in the batch in the early stage of the synthesis (i.e., the so-called one-pot method).[9,24,36−38] The latter strategy requires the use of two Si precursors: a coupling agent to anchor silicon to polymeric chains, usually APTES, and the main source of the silica network, usually TEOS. A synthetic procedure recently proposed allowed obtaining nanoenvironments formed by silica crystalline multisheets dispersed in a DGEBA epoxy matrix, keeping the TEOS/APTES molar ratio equal to 2.3.[12,39] The challenge faced in the current work was the incorporation of phosphorus moieties in silica-based nanodomains, which competes with its tendency to react with the epoxy group, using phosphoric acid as a P precursor. The high reactivity of H_3PO_4 toward DGEBA, the presence of water, and the intrinsic hydrolytic instability of Si−O−P bonds made this task very challenging. We faced these issues by separating the synthetic route into two steps (see Scheme 1). In the first step, the hydrolysis of Si precursors in polar nanoenvironments occurs almost completely as it is driven by the operating temperature (80 °C) and APTES. Then, the addition of the H_3PO_4 solution in ethanol at room temperature allows the simultaneous incorporation of phosphorus in both epoxy chains and nanodomains. Finally, the addition of the curing agent freezes the further evolution of the system. Keeping the TEOS/APTES molar ratio equal to 2, different hybrid nanocomposites were obtained, changing the Si/P molar ratio from 1.0 to 4.0 (see Table 1). Moreover, a silicon-free sample (i.e., EPO_1P) was also synthesized for comparative purposes.

The designed modification route complies with several principles of green chemistry, as the reagents and solvents are safe and easy to handle, no additives or catalysts are needed, the silicon and phosphorus contained in the precursors are completely incorporated into the final product, and the process occurs in a single batch by simple heating in mild conditions.

Table 1. Nominal Composition of Prepared Epoxy Nanocomposites

sample	Si (wt %)	P (wt %)	Si/P (mol/mol)
EPO_1Si1P	0.90	1.0	1.0
EPO_1Si0.5P	0.90	0.50	2.0
EPO_2Si1P	1.8	1.0	2.0
EPO_3Si1P	2.7	1.0	3.0
EPO_4Si1P	3.6	1.0	4.0
EPO_1P	0.0	1.0	

^{29}Si, ^{31}P, and ^{13}C solid-state NMR spectra were recorded on all prepared materials. Cross-linking in the ^{13}C, ^{29}Si, and ^{31}P NMR spectra can be denoted by the T_N, Q_N, and Q'_N notation, where T_N, Q_N, and Q'_N stand for $RSi(OX)_N(OH)_{3-N}$, $Si(OX)_N(OH)_{4-N}$, and $OP(OX)_N(OH)_{3-N}$, respectively (with R = alkyl group and X = C, Si, or P). ^{29}Si cross-polarization (CP) MAS experiments were carried out due to the long T_1 relaxation time of ^{29}Si in the solid state. Although it is well known that experiments in cross-polarization mode mainly reveal signals of silicon atoms that are directly linked and/or dipolar coupled to hydrogen, thus precluding a quantitative analysis, some considerations can be drawn. In Figure S1, the typical ^{29}Si CP-MAS deconvoluted spectra are shown. Two groups of resonances are detected in all spectra, which correspond to Q and T silicon sites.[40] A very broad and complex peak appears in the range from −110 to −90 ppm, which can be fitted with three lines centered approximately at −91, −100, and −109 ppm. These resonances can be ascribed to silicon atoms (structured as $(Si\text{-}O)_2Si(OH)_2$) characterized by geminal silanols and labeled as Q_2, at −91 ppm; silicon atoms linked to only one hydroxyl group, $(Si\text{-}O)_3Si\text{-}OH$, labeled as Q_3, at −100 ppm; silicon atoms connected to four other silicon tetrahedra (i.e., $Si(O\text{-}Si)_4$), labeled as Q_4, at −109 ppm. The other group of resonances also appears as a complex and broad peak in the range from −55 to −70 ppm. It was deconvolved in three signals that refer to silicon atoms of the APTES molecules. In particular, the peak at −55 ppm was assigned to silicon sites, in which one ethoxy group for each APTES molecule is involved in the condensation reaction to form an organosiloxane network labeled as T_1. The resonances at −64 and −70 ppm are assigned to silicon atoms, in which two (T_2) or three (T_3) ethoxy groups are condensed to form the network, respectively. Comparing the spectra, a progressive increase in the Q/T ratio can be observed: it can be correlated to the increased silicon content in the epoxy materials (Figure S1 and Table 2). At a higher silicon content, residual unreacted APTES can be highlighted by the presence of the signal at −44 ppm (Figure S1d,e).

To examine the chemical environment of phosphorus and provide direct evidence for Si−O−P bond formation, ^{31}P direct polarization (DP) NMR measurements were performed; the relative deconvolved spectra are reported in Figure S2. All ^{31}P spectra present a main, complex resonance centered at about 4.2 ppm, ascribable to the formation of organic phosphoester groups. This resonance can be fitted by two lines, at approximately 4.5 and 2.8 ppm, and assigned to mono- and diester groups, respectively (i.e., Q'_1 and Q'_2 P sites), formed by the reaction of P−OH moieties of phosphoric acid with one or two epoxy rings of DGEBA.[41,42] Comparing the area of these peaks, the diester formation seems to be favored (Table 2), which points out the possible role of phosphorus as a co-crosslinker of the epoxy resin.[41,43] A representative

https://doi.org/10.1021/acsanm.3c00590
ACS Appl. Nano Mater. 2023, 6, 7422−7435

Table 2. Chemical Shifts, δ (ppm), Estimated Relative Intensities, I, and Full Width at Half-Maximum, FWHM (ppm), Calculated from Line Fitting of the ^{29}Si CP NMR and ^{31}P DP NMR Spectra[a]

sample	δ ^{29}Si (ppm)	I (−)	FWHM (ppm)	δ ^{31}P (ppm)	I (−)	FWHM (ppm)
EPO_1Si0.5P	−44.0	0.03	3.2	4.46	0.10	1.62
	−55.5	0.07	8.6	2.80	0.79	5.62
	−64.4	0.41	7.5	−6.50	0.11	7.03
	−70.6	0.09	6.2			
	−91.0	0.07	12.0			
	−99.7	0.17	6.8			
	−108.6	0.16	9.0			
EPO_1Si1P	−55.5	0.03	6.1	4.49	0.13	1.75
	−64.7	0.51	7.4	2.60	0.76	5.62
	−70.6	0.15	6.0	−6.26	0.11	8.00
	−91.1	0.03	7.5			
	−100.3	0.17	8.0			
	−108.9	0.11	7.7			
EPO_2Si1P	−43.7	0.02	1.7	4.58	0.10	1.66
	−54.0	0.06	8.6	2.71	0.75	5.72
	−64.4	0.44	7.8	−6.56	0.15	7.75
	−71.1	0.10	7.2			
	−91.9	0.06	9.9			
	−100.1	0.14	5.3			
	−108.9	0.19	10.0			
EPO_3Si1P	−44.8	0.04	3.3	4.42	0.19	1.84
	−55.5	0.06	10.2	2.82	0.71	5.61
	−64.7	0.29	7.4	−6.37	0.10	7.45
	−70.2	0.14	9.3			
	−91.1	0.08	11.1			
	−100.0	0.22	7.4			
	−108.8	0.17	8.4			
EPO_4Si1P	−44.3	0.14	3.4	4.41	0.20	1.85
	−55.1	0.09	11.3	2.89	0.70	5.33
	−64.2	0.25	7.3	−6.40	0.10	7.56
	−70.6	0.06	9.3			
	−92.0	0.09	11.3			
	−99.7	0.22	7.7			
	−109.0	0.15	7.5			
EPO_1P				4.05	0.14	1.36
				2.69	0.86	5.50

[a]Standard errors for peak position (δ) are less than 0.6 ppm (^{29}Si) and 0.03 ppm (^{31}P); for FWHM, they are less than 1 ppm (^{29}Si) and 0.07 ppm (^{31}P); for the relative intensities, they are less than 0.1 (^{29}Si) and 0.02 (^{31}P). Higher errors for ^{29}Si parameters are due to the low signal/noise ratio in ^{29}Si spectra.

illustration of the envisaged inorganic−organic structure of the studied nanocomposites based on the NMR data is shown in Scheme 1. It can be noticed that the relative diester/monoester ratio decreases with increasing the silicon content (Table 2), possibly because a higher fraction of DGEBA molecules is functionalized with APTES and thus involved in the formation of the hybrid epoxy−silica structures. Consequently, the number of oxirane rings available to react with phosphoric acid becomes lower.

Interestingly, an additional broad peak was detected and approximately centered at about −6 ppm in all materials containing silicon (Figures 1 and S2a−e). This resonance could be compatible with the formation of mixed Si−O−P structures even if these latter in inorganic systems produce signals in a range from −40 to −10 ppm.[30,44] The observed downfield shift suggests the involvement of phosphoesters in the formation of the Si−O−P structures (for example, mono- or diphosphate groups condensed with a silanol, giving Q'_2 or Q'_3 sites, respectively, as depicted in Scheme 1). To strengthen this assignment, the ^{31}P DP spectrum of an epoxy-based material containing only phosphorus (EPO_1P) was also acquired. In the absence of Si, the very high reactivity of phosphoric acid toward the epoxy resin gives rise only to mono- and diester groups, and the lack of resonance at −6 ppm allows for the unambiguous assignment of this peak to the formation of Si−O−P (Figures 1 and S2f). It should be underlined that the formation of Si−O−P bonds in the epoxy-based network should result in the appearance in ^{29}Si solid-state NMR spectra of signals in the range from −110 to −120 ppm, even if in the presence of a small amount of such bonds just a slight shift toward upfield in the resonance position might be seen.[30,44] However, due to the wide lines of silicon and the low signal-to-noise ratio in the spectra, as well as the lower number of Si−O−P links compared to Q and T sites, the presence of such resonances cannot be observed.

Finally, ^{13}C spectra (Figure S3) do not evidence any significant difference in the main carbon resonances between

https://doi.org/10.1021/acsanm.3c00590
ACS Appl. Nano Mater. 2023, 6, 7422−7435

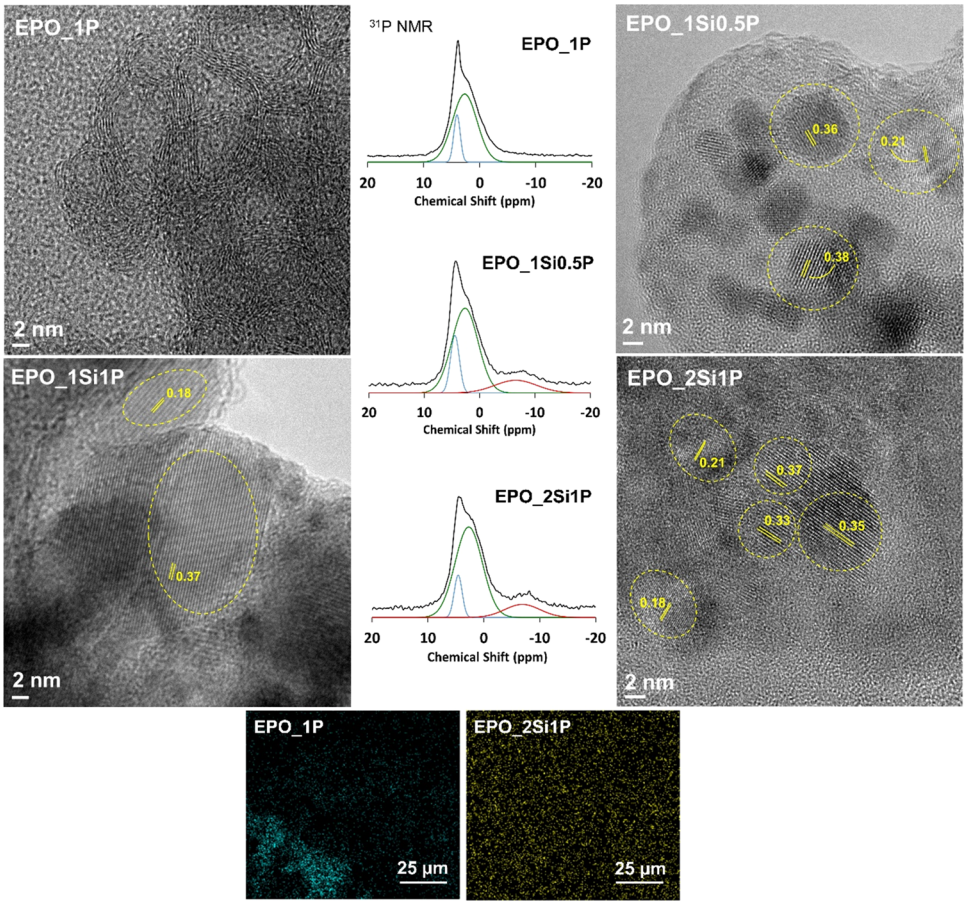

Figure 1. HRTEM images, ^{31}P solid-state NMR spectra, and EDX maps of representative epoxy composites. The HRTEM of EPO_1Si0.5P, EPO_1Si1P, and EPO_2Si1P hybrid samples show nanocrystals with lamellar morphology and two different sheet thicknesses, whereas EPO_1P displays a wormlike morphology. In the ^{31}P solid-state NMR spectra, the fitting curves are reported (green peaks assigned to mono- and diphosphates, red peak attributed to P−O-Si sites). The EDX maps show the phosphorus distribution for EPO_1P and EPO_2Si1P.

the nanocomposites and the neat epoxy system prepared as a reference, likely due to the low amount of Si and P added.

ATR-FTIR spectra (Figure S4) confirm the consistency of the nanocomposite structure. In all of the analyzed samples, the band at 914 cm^{-1}, corresponding to the stretching of the oxirane rings of bare DGEBA, disappeared, and a broad O−H stretching band around 3400 cm^{-1} showed up, confirming the effective and complete curing of the resin. The spectra of hybrid nanocomposites show a band centered at 1085 cm^{-1}, characteristic of Si−O bond stretching, whose intensity grows with increasing Si content. Phosphorus-related features can be seen as weak stretching bands at the same wavenumber (P−O bonds around 1085 cm^{-1}) and at 960 cm^{-1} (attributed to P−O−C linkages),[45] whereas other bands associated with silicate and phosphate units are not detectable, being overlapped with intense bands of the resin network.[46]

According to the above NMR analysis, the intensity of the resonance assigned to Si−O−P bonds does not change significantly with the Si/P content, reaching the highest value in EPO_2Si1P (see Table 2), excluding the possibility of forming more Si−O−P bonds with more silicon added. Consequently, the samples with the higher Si content were not further investigated.

The morphology of hybrid nanocomposites is displayed in Figure 1, where some ^{31}P solid-state NMR spectra are also reported to highlight the relationship between the morphology and distribution of P units. The lack of silicon does not allow the formation of crystalline nanostructures in EPO_1P. The high reactivity of H_3PO_3 toward the oxirane rings of DGEBA causes the generation of mono- and diester groups, giving rise to a peculiar one-dimensional wormlike morphology (Figures 1 and S5). Crystalline nanoenvironments start to appear in the presence of silicon (see Figure 1 and additional HRTEM images in Figures S6−S8), confirming that the adopted synthesis procedure accounts for the occurrence of suitable conditions for the growth of SiO_2 lamellar nanocrystals, similarly to the liquid crystal templating (LCT) technique, but without the addition of amphiphilic templates/surfactants.[34,47−50] In this case, the polymer matrix acts as an apolar medium, in which the polar nanodroplets, rich in the inorganic component, are uniformly dispersed, like inverse micelles. The presence of phosphorus does not alter the general scheme of the synthesis but strongly affects the growth of lamellar silica nanocrystals. Two different sheet thicknesses are clearly seen for EPO_1Si0.5P, EPO_1Si1P, and EPO_2Si1P hybrid nanocomposites, namely, 0.36 ± 0.03 nm (**d1**) and 0.20 ± 0.02 nm (**d2**). The **d1** is very close to the previously observed values for epoxy−silica hybrids containing no P[12] and for nanocrystals obtained by LCT.[34,47−51] The thinner interlayer distance **d2** is likely due to the presence of phosphorus in crystalline nanoenvironments that originate the formation of Si−O−P bonds in agreement with the solid-state NMR analysis (Figure 1).

https://doi.org/10.1021/acsanm.3c00590
ACS Appl. Nano Mater. 2023, 6, 7422−7435

Scheme 2. Overall Mechanism Proposed for the Two-Step Synthetic Route[a]

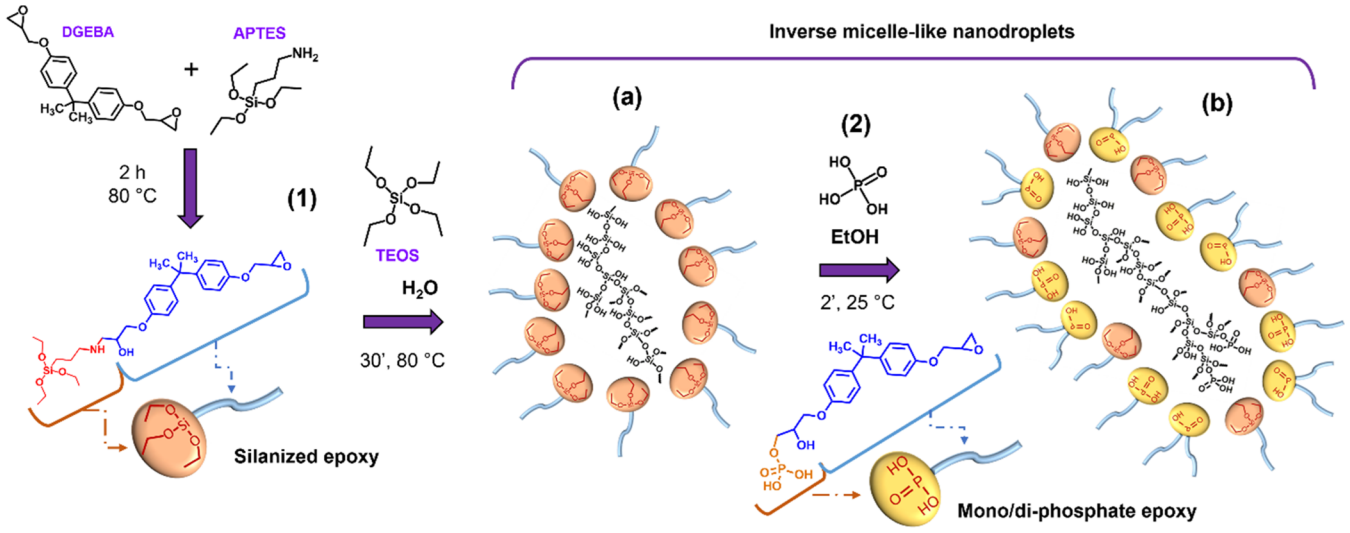

[a]A hybrid epoxy−silica matrix is obtained by hydrolyzing a mixture of DGEBA, APTES, and TEOS, followed by the addition of phosphoric acid. Both silane-epoxy and phosphate-epoxy compounds have amphiphilic characteristics and form nanodomains resembling inverse micelles. These represent suitable nanoenvironments for the stabilization of Si−O−P bonds and the embryonic growth of a co-continuous organic−inorganic network consisting of lamellar silica nanocrystals and P-moieties linked to the polymer matrix.

Despite their hydrolytic instability,[30,52] the establishment of these bonds occurs in the hybrid nanocomposites because the adopted synthesis strategy allows controlling the reactivity of both water and H_3PO_4. In the first step of the synthesis, the addition of Si precursors to the epoxy resin causes a phase separation at the nanoscale level, with the formation of an inverse micelle system, in which polar nanodomains act as nanoreactors for the hydrolysis and condensation of TEOS,[53] originating silica lamellar nanocrystals[51] in agreement with the Q unit distribution revealed by NMR analysis. In the subsequent step, the high reactivity of phosphoric acid toward the oxirane rings of DGEBA is partially counteracted by its tendency to diffuse into nanodomains, which is driven by its physicochemical affinity with the hydrophilic inner environment of nanodomains (see Scheme 2). In these nanoreactors, the Si−O−P bonds are stable mainly because the quantity of available water, whose total amount accounts for the H_2O/(APTES+TEOS) = 2.7 molar ratio adopted, the water produced by condensation of silanol groups and the small amount already present in 85 wt % H_3PO_4, is insufficient to complete their hydrolysis as the majority of water is consumed in the first step for the hydrolysis of Si precursors. The trend of the intensity of the resonance associated with these bonds (δ at about −6 ppm) as a function of the P content supports this interpretation. Further, it does not change doubling the phosphorus content to achieve that of silicon (EPO_1Si1P), while it slightly increases doubling the silicon content with respect to phosphorus (EPO_2Si1P, see Table 2).

This suggests that the amount of Si−O−P bonds is mainly limited by the P diffusion into nanodomains and, to a lesser extent, by the total number of nanodomains, which is mainly controlled by the Si content. On the other hand, the intensity of this resonance does not change, increasing Si and keeping the P content constant (Table 2).

The distribution of nanodomain size derived from the analysis of TEM images is displayed in Figures S9 and S10. For each interlayer distance, a similar trend with the Si and P contents was observed. Doubling the phosphorus content, being equal to that of silicon, produces a wider distribution of the mean size of nanodomains with the appearance of nanocrystals ranging from 25 to 35 nm. Conversely, a slight narrowing of the size distribution was observed, doubling the silicon content while keeping the phosphorus content constant (Figures S9 and S10).

The different P distribution in the epoxy matrix for the EPO_1P and EPO_2Si1P samples is further confirmed by SEM-EDX maps displayed in Figure 1. In the former sample, P appears locally concentrated, whereas the presence of silicon allows a uniform P distribution on a microscopic scale, corroborating the occurrence of Si−P interactions.

2.2. Thermal and Fire Behavior. DSC curves of the neat resin and hybrid nanocomposites are displayed in Figure S11. In the first heating ramp, no exothermic peak is seen in the examined temperature range for all of the samples, thus confirming the completeness of the curing process in agreement with ATR-IR analyses.

Dynamic mechanical analysis was employed for evaluating the viscoelastic response of the material as a function of temperature. Glass transition temperature (Tg) values were evaluated as the temperatures corresponding to the maximum of tan δ curves (Figure 2a). EPO exhibits a symmetric and narrow curve with the highest tan δ values (tan δ peak at 94 °C) in comparison with the other samples, indicating that the application of a load to EPO can be easily dissipated by energy dissipation mechanisms such as segmental motions, while another part of the load is stored in the material and will be released upon removal of the load.[54]

EPO_1P and hybrid nanocomposites show asymmetric and wider tan δ curves than EPO due to two co-continuous phases with different chain mobilities and a broad distribution of relaxation phenomena.[11,38,55] In EPO_1P, two well-resolved maxima are seen (Tg_1 = 94 °C, Tg_2 = 107 °C), in agreement with the structural and morphological analysis reported above. The interconnected wormlike structure formed by mono- and diphosphate epoxy chains may stiffen the epoxy system through the establishment of hydrogen bonds between

https://doi.org/10.1021/acsanm.3c00590
ACS Appl. Nano Mater. 2023, 6, 7422−7435

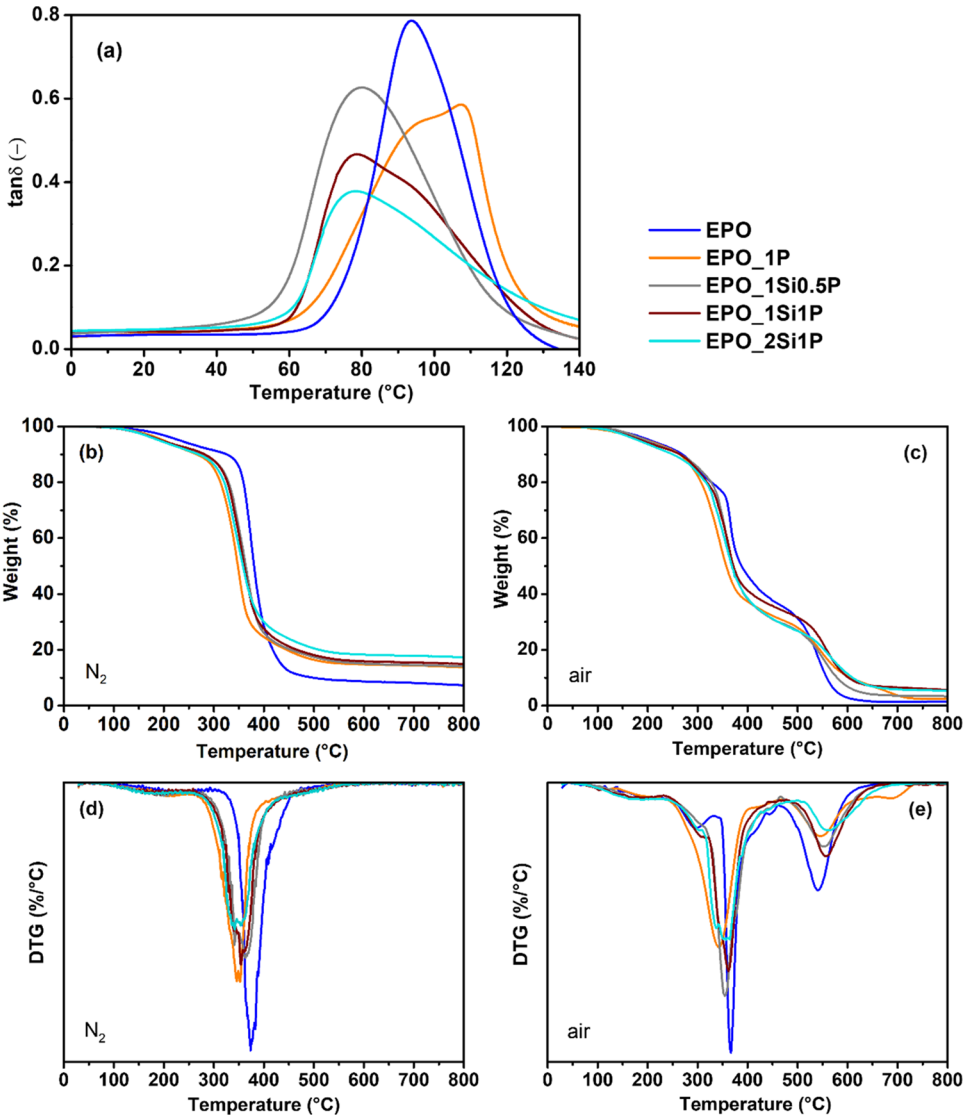

Figure 2. (a) Mechanical damping factor (tan δ) of pristine resin (EPO), modified resin with phosphorus (EPO_1P), and hybrid nanocomposites (EPO_1Si0.5P, EPO_1Si1P, and EPO_2Si1P), collected as a function of temperature. (b, c) TG curves and (d, e) DTG curves of the same samples recorded under nitrogen and air, respectively.

phosphate-based moieties and hydroxyl groups formed during the cross-linking process, exhibiting a second glass transition temperature (Tg_2).[24,42,56]

In hybrid nanocomposites, a maximum of tan δ occurs at 79 °C (Tg_1), together with a small shoulder at about 94 °C (Tg_2), as shown in Figure 2a. This indicates the existence of two co-continuous phases, as discussed above. The crystalline nanodomains limit the molecular motion of polymer chains, resulting in a more elastic response of the material. The presence of crystalline domains negatively affects the mobility of polymer chains by disturbing the inter-chain interactions and curing in the polymer matrix. Thus, the material has a lower ability to dissipate the energy received from a load application.[57] These observations are in agreement with the storage moduli (E') collected as a function of the temperature and reported in Figure S12. In particular, it is possible to note that EPO_2Si1P shows the lowest values of E' in the glassy state region, likely due to the presence of dangling segments causing a network loosening effect with respect to the other nanocomposites, for which E' values are quite similar. Therefore, a limited content of the inorganic phase does not significantly affect the dynamic-mechanic behavior of the resulting hybrids. Similar results were already observed in previous research works,[11,19,21] where the incorporation of in situ silica-based phases led to a decrease in the storage modulus. However, based on the DMA characterization, it may be argued that the in situ generation of Si/P nanostructures only marginally worsens the mechanical behavior of the materials.

TG curves recorded in nitrogen (Figure 2b) and air (Figure 2c) and their first derivative (Figure 2d,e) show that both pristine EPO and hybrid nanocomposites decompose through a mechanism similar to that described for epoxy resins cured with aliphatic amines.[24,58,59] The relatively low initial degradation temperatures (see Figure 2 and T5% values in Table S1) observed in EPO are comparable with those found for epoxy-based systems prepared by using similar curing cycles and showing Tg values in the same range.[19,60] In the nitrogen atmosphere, the main degradation step occurs at around 350 °C, as for epoxy aliphatic systems.[20,58] As

https://doi.org/10.1021/acsanm.3c00590
ACS Appl. Nano Mater. 2023, 6, 7422−7435

Table 3. Pyrolysis-Combustion Flow Calorimeter Data for All of the Investigated Samples[a]

sample	THR (kJ/g)	ΔTHR (%)	HRC (J/g K)	ΔHRC (%)	pkHRR (W/g)	ΔpkHRR (%)	residue (wt %)
EPO	28 ± 0.4		397 ± 25		401 ± 24		5 ± 0.5
EPO_1P	25 ± 1.1	−10.7	331 ± 4.1	−16.6	329 ± 8.1	−9.2	13 ± 0.4
EPO_1Si0.5P	24 ± 0.5	−14.2	335 ± 18	−15.6	340 ± 14	−15.2	13 ± 0.9
EPO_1Si1P	23 ± 0.5	−17.8	322 ± 19	−18.8	324 ± 18	−19.2	16 ± 0.4
EPO_2Si1P	24 ± 0.4	−14.2	296 ± 9.8	−25.4	294 ± 6.3	−26.6	15 ± 0.7

[a]**THR** = Total heat release, **HRC** = heat release capacity, and **pkHRR** = peak of heat release rate.

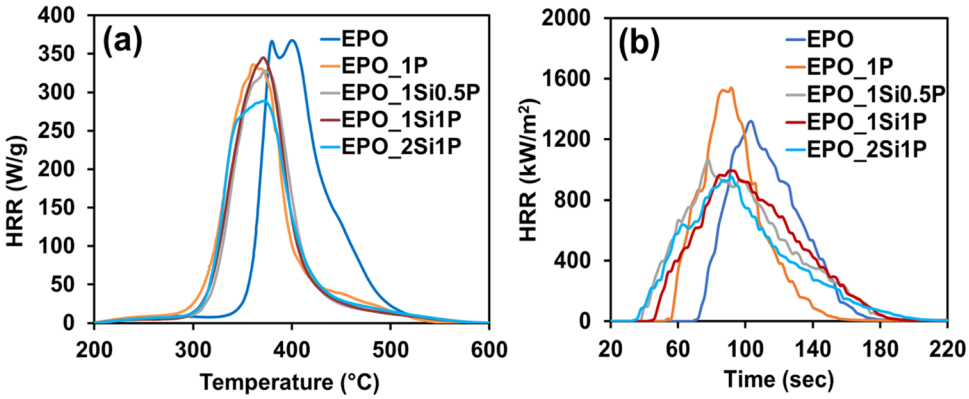

Figure 3. Heat release rate (HRR) of pristine resin (EPO), modified resin with phosphorus (EPO_1P), and hybrid nanocomposites (EPO_1Si0.5P, EPO_1Si1P, and EPO_2Si1P) measured by PCFC (a) and cone calorimetry (b).

displayed in Table S1, the mass loss of EPO_1P and hybrid nanocomposites in both nitrogen and air is anticipated with respect to EPO because of two main reasons: (i) the presence of nanodomains containing lamellar silica and phosphorus-based moieties and (ii) the generation of acidic phosphorus species via decomposition of phosphate groups (i.e., monophosphate and diphosphate species).[61] The presence of P and Si confers acidic characteristics to the epoxy matrix, which influence the kinetics of the pyrolysis process, catalyzing the reactions responsible for the release of gaseous species. However, this effect has a lower impact on the thermal behavior in air, where the mass losses of hybrid nanocomposites in the first (<400 °C) and second steps (400−600 °C) do not show a significant variation with respect to the pristine resin (Table S1). On the other hand, the hybrid nanocomposites exhibit a lower mass loss rate in the second step than EPO (Figure 2e), which suggests an improved thermo-oxidative stability of such samples and the formation of a more stable aromatic char at high temperatures.[62] The higher residue in air exhibited by hybrid nanocomposites with respect to EPO (Table S1) supports the above interpretation, confirming the formation of a more resistant char toward oxidative processes.[17,63] EPO_2Si1P shows the highest residues at 800 °C in both nitrogen and air atmospheres and, thus, the highest overall thermal stability. In agreement with NMR analysis, this sample shows the highest percentage of Si−O−P bonds, which play a key role in the production of a very stable char in the condensed phase.[24,41] Therefore, the TG results shed some light on the condensed phase mechanisms that occur during the degradation of hybrid nanocomposites, revealing an improved thermal behavior compared to the epoxy resin embedding phosphorus-based moieties only.

The flammability of pristine EPO and its hybrid nanocomposites was investigated by UL94 vertical flame spread tests and limiting oxygen index measurements (Table S2). All samples burned up completely to the holding clamp in a very short time and thus could not be classified, though their burning resulted in the production of a very coherent char. The hybrid nanocomposites produce a continuous char due to the presence of Si and P in the epoxy matrix, which increases the melt viscosity of the burning system.[16,17] However, the char produced by EPO_1P was brittle, its backbone flaked, and dripping phenomena were observed just after the flame ignition. EPO_1Si0.5P, EPO_1Si1P, and EPO_2Si1P burned without any dripping and ignition of cotton batting. The absence of dripping phenomena is highly desirable, as the drops released during the combustion of a melting polymer system could trigger a second flame source during a fire scenario. LOI represents the measure of the minimum percentage of oxygen that is required in an O_2/N_2 mixture to support the candle-like combustion of the polymer-based material. Table S2 shows that moving from the neat epoxy to the Si/P−epoxy hybrid nanocomposites, the minimum oxygen concentration that is necessary to sustain stable combustion of the specimens after ignition slightly increases, which means that in situ modified samples have a lower tendency in capturing the candle-like flame compared to virgin resin. Due to a higher flammability resistance, the flame released from Si/P−epoxy hybrid nanocomposites provides lower heat flux than EPO and EPO_1P during the LOI measurements. These results agree with the main outcomes of UL94 vertical flame spread tests.

PCFC and cone calorimetry tests in forced combustion conditions allow for the determination of different thermal and smoke parameters, revealing additional aspects of the fire behavior of the synthesized nanocomposites. The cone calorimetry tests are performed in an air atmosphere and simulate a fire scenario starting from a heat radiation source, where the flammable gases undergo ignition by the application of a spark. Conversely, PCFC can be considered a nonflaming test, as the sample undergoes pyrolysis in an inert gas stream,

https://doi.org/10.1021/acsanm.3c00590
ACS Appl. Nano Mater. 2023, 6, 7422−7435

Table 4. Results from Cone Calorimetry Tests for the Investigated Samples[a]

sample	TTI (s)	ΔTTI (%)	TTP (s)	ΔTTP (%)	pkHRR (kW/m^2)	ΔpkHRR (%)	THR (MJ/m^2)	ΔTHR (%)	residue (wt %)
EPO	62 ± 3		100 ± 2		1313 ± 384		65 ± 3		3 ± 0.7
EPO_1P	44 ± 1	−29.1	92 ± 3	−8.1	1536 ± 81	+16.9	64 ± 2	−1.5	8 ± 0.5
EPO_1Si0.5P	38 ± 6	−38.7	91 ± 1	−9.3	1066 ± 122	−18.8	75 ± 6	+15.3	9 ± 0.4
EPO_1Si1P	36 ± 4	−41.9	94 ± 4	−6.2	993 ± 73	−24.3	71 ± 10	+9.1	10 ± 0.3
EPO_2Si1P	26 ± 5	−58.1	93 ± 2	−7.1	949 ± 108	−27.7	63 ± 7	−3.2	12 ± 0.7

[a]**TTI** = Time to ignition, **TTFO** = time to flame out, **THR** = total heat release, **MLR** = mass loss rate, **HRR** = heat release rate, **TTP** = time to peak, **pkHRR** = peak of heat release rate.

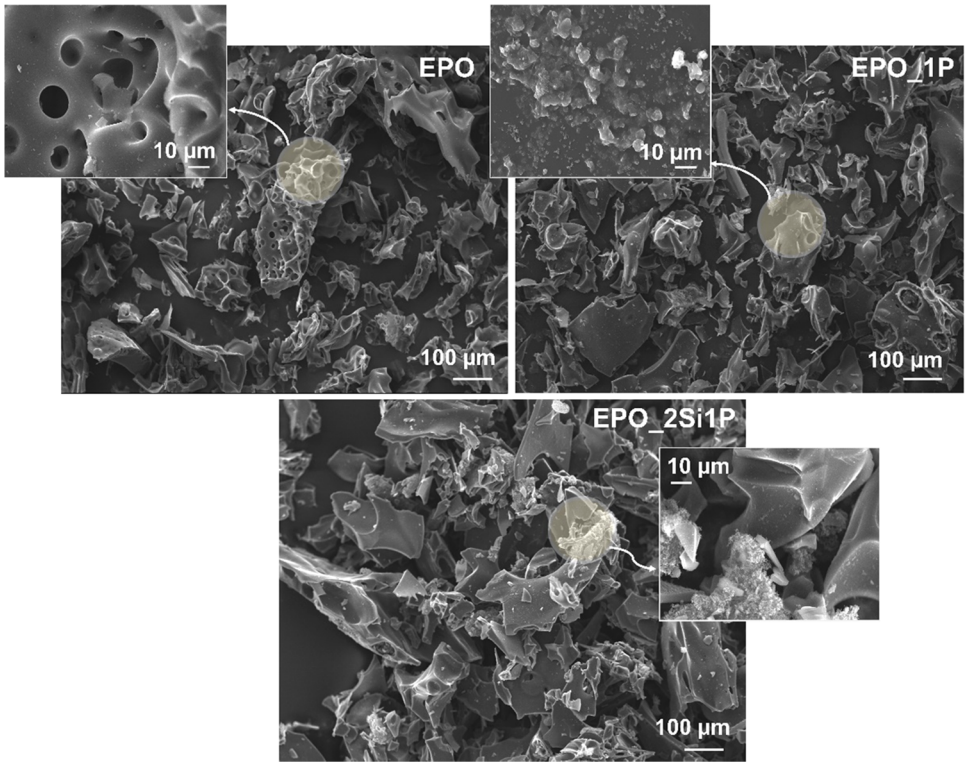

Figure 4. Typical SEM images of the residual char obtained after cone calorimetry tests of EPO, EPO_1P, and EPO_2Si1P samples.

and subsequently, the volatiles are oxidated at high-temperature in a separate chamber.[64,65] The combined use of PCFC and cone calorimetry allows for obtaining a complete overview of the flame-retardant mechanisms exerted by flame-retarded systems during combustion.

PCFC data are summarized in Table 3; the related heat release rate (HRR) vs temperature curves are displayed in Figure 3a. Compared to EPO, all of the hybrid nanocomposites exhibited decreased THR and pkHRR values, as well as increased residues at the end of the tests. These findings confirm the flame-retardant action exerted by the hybrid moieties, which are able to protect the polymer network during its pyrolysis, slowing down the release of flammable gaseous products.

The flame-retardant effectiveness of the hybrid structures was further supported by the results from cone calorimetry tests (Table 4 and Figure 3b). First, it is noteworthy that all of the hybrid nanocomposites show an anticipation of time to ignition (TTI, Table 4) compared to pristine EPO; in particular, the lowest TTI values were measured for EPO_1Si1P and EPO_2Si1P (36 and 26 s, respectively, vs 62 s for the EPO sample). This finding can be attributed to the increased acidic characteristics of the hybrid matrices, which favor the dehydration processes and in turn accelerate the char formation during combustion. Furthermore, the shape of the HRR curves for EPO_1Si0.5P, EPO_1Si1P, and EPO_2Si1P is broader and more flattened than that of EPO, indicating a slower heat release over a longer time span (Figure 3b).[20,66] Again, the presence of a Si−O−P network leads to an increased overall thermal stability and the formation of a hybrid coherent char (Figure 4), acting as a thermal insulating barrier at the boundary phase during combustion. This char is enriched of inorganic components (i.e., Si−O−P substructures), as shown through the comparison of the EDX analyses carried out on the hybrid nanocomposites before and after cone calorimetry tests (Table S3). Besides, EPO_1P exhibits an HRR curve narrower and higher (ΔpkHRR = +16.9%, Table 4) than that of EPO, which means a large amount of heat released in a short period of time, despite the larger amount of char produced by EPO_1P with respect to EPO (Table 4). The worse fire behavior of EPO and EPO_1P may be ascribed to different features of the char obtained after cone calorimetry tests. The char morphology of EPO appears less compact (i.e., with holes and cracks) and fragmented (Figure 4), resulting quite ineffective in slowing down the heat and mass transfer during the flaming combustion. On the other

https://doi.org/10.1021/acsanm.3c00590
ACS Appl. Nano Mater. 2023, 6, 7422−7435

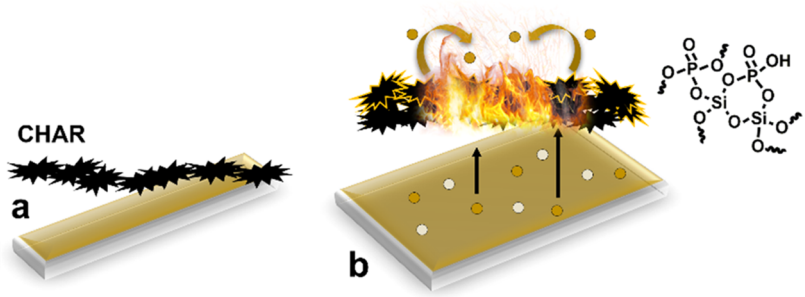

Figure 5. Simplified representation of flame-retardant mechanisms occurring during the combustion of hybrid nanocomposites in an oxygen atmosphere. In particular: (a) represents the pristine epoxy sample and (b) the hybrid Si/P nanocomposites. The brown region indicates the hot bulk polymer matrix with rising bubbles (white circles). The black arrows display the direction of flammable gases. The yellow circles illustrate the in situ generated silica nanoparticles dragged from the inner of the matrix to the char surface. The yellow border line characterizing the black char represents the ceramic silica layer. The chemical formula shows the P−O-Si polymeric substructures and thus the chemical composition of the respective residue surface.

hand, the forced combustion of EPO_1P implies the decomposition of mono- and diphosphate groups, which generates phosphorus-based acidic compounds able to catalyze the degradation of the polymer matrix and boost the release of flammable volatiles to the flame in the gas phase.[67]

Such release of pyrolytic gases, rising from the condensed phase, occurs quickly and exerts enough pressure to break the coherent and continuous wall of char forming during the combustion of EPO_1P (Figure 4). This phenomenon, which was observed during cone calorimetry and UL94 vertical burning tests, could contribute to rapidly increase the heat transfer, hence resulting in a huge amount of heat released in a short time (Figure 3b).

The progressive decrease of the CO/CO_2 ratio with increasing the Si/P content, together with the increase of residual masses obtained from cone calorimetry tests (Table S4) and the high retention of both P and Si in the char (Table S3), further confirm that the flame-retardant mechanism occurs in the condensed phase of the hybrid nanocomposites.[68] Particularly, the CO/CO_2 ratio changes from 0.4 for EPO to 0.1 for EPO_2Si1P, which is characterized by the largest amount of Si−O−P bonds in the polymer matrix, suggesting the key role played by these bonds to give a condensed phase mechanism.

More in detail, during the combustion of hybrid nanocomposites, the silanol groups of Si−O−Si polymeric species, belonging to the organic−inorganic co-continuous network, condense with the decomposition products of mono- and diphosphate groups (i.e., polyphosphoric acids) leading to the formation of P−O-Si polymeric substructures on a very abundant char. This latter can provide an effective ceramic thermal shield, limiting the heat exchange and the transfer of oxygen between the gas phase and the polymer matrix. Figure 5 shows a simplified representation of the flame-retardant mechanism playing a key role during the combustion of the hybrid nanocomposites.

Table S4 shows for all of the investigated samples an increase in the total amount of released smoke and smoke extension area, which is linked to higher CO and CO_2 yields compared with EPO. It is reported in the literature that the use of inorganic flame-retardant systems is not able to reduce smoke production, for which the use of specific smoke suppressants (e.g., metal oxides, phosphate-based salts, etc.) is required. Inorganic flame-retardant systems (e.g., silica nanoparticles, montmorillonite, etc.) improve the fire behavior of polymer systems through condensed phase mechanisms, which do not exert any beneficial effect on the amount of high molecular weight combustion products formed in the gas-phase combustion process.[67,69]

3. CONCLUSIONS

A synthetic strategy was established to produce hybrid Si/P−epoxy-based nanocomposites, in which the inorganic component is uniformly dispersed at the nanometric size in the polymeric matrix. This is obtained by means of a two-step procedure involving: (i) the formation of silica lamellar nanocrystals as a result of the hydrolysis reactions of TEOS occurring within polar nanodomains embedded into an inverse micelle system originating from phase separation phenomena and (ii) the formation of stable Si−O−P structures in the inner of silica nanodomains because of the balance of two counteracting effects (i.e., the reactivity of phosphoric acid toward the oxirane rings of the epoxy resin and its tendency to diffuse into nanodomains, whose total number is mainly controlled by the Si amount). This chemical modification strategy represents an environmentally sustainable process employing inexpensive and safe reagents and solvents and mild temperature conditions. The resulting hybrid Si/P nanocomposites are formed by two co-continuous phases, i.e., P-modified silica nanocrystals covalently interconnected with epoxy chains. Their peculiar morphology accounts for interesting flame-retardant features, even with Si and P contents around 1 wt %: no dripping phenomena during UL94 tests (though the materials were all not classifiable), the formation of a large amount of coherent and continuous char both in nitrogen and air atmospheres, and the low CO/CO_2 ratio in the smokes obtained by the cone calorimetry tests, indicating a prevalent condensed phase mechanism.

The above findings suggest considering these hybrid epoxy systems as suitable matrices for the design of composites with enhanced flame-retardant features in the presence of very low loadings of flame-retardant and therefore with a limited detrimental impact on the mechanical performances of the final products. The intrinsic fire resistance of these materials opens some interesting perspectives for their development and application in several industrial areas, for example, in flame-retardant coatings, sealants, components of electronic circuit board substrates, or fiber-reinforced structural composites.

https://doi.org/10.1021/acsanm.3c00590
ACS Appl. Nano Mater. 2023, 6, 7422−7435

4. EXPERIMENTAL SECTION

4.1. Synthesis of the Nanocomposites. 3-Aminopropyltriethoxysilane (APTES, >98%), bisphenol A diglycidyl ether (DGEBA), tetraethyl orthosilicate (TEOS, >99%), phosphoric acid (H_3PO_4, 85 wt % solution in water), deionized water, ethanol (ACS reagent, anhydrous), and isophorone diamine (IDA) were used as starting materials. APTES, TEOS, phosphoric acid solution, and ethanol were purchased from Sigma-Aldrich (Switzerland). DEGBA and IDA were purchased as a two-component epoxy resin system (SX10) from MATES S.r.l. (Milan, Italy) and used as received. The synthetic procedure starts with the formation of the hybrid epoxy−silica chains according to a procedure previously proposed.[20,70] Briefly, DGEBA, APTES, TEOS, and water were mixed at 80 °C for 2 h with the following molar ratios: DGEBA/TEOS ranging from 2.7 to 9.8; TEOS/APTES = 2; and H_2O/(APTES+TEOS) = 2.7. The system was subsequently cooled to room temperature, and a solution of phosphoric acid and ethanol (EtOH/H_3PO_4 ranging from 0.7 to 1.3 mol/mol) was added dropwise into the reaction vessel under stirring. Then, IDA (26 wt % with respect to DGEBA, corresponding to an IDA/DGEBA molar ratio of 0.5, so to an amine/oxirane groups equivalent ratio of 0.5) was added and mixed shortly before pouring the resulting mixture into the mold. The system was cured at 60 °C for 24 h and then post-cured at 80 °C for 4 h.

Samples of neat epoxy resin and P-modified resin were prepared as a reference, the former by mixing only DGEBA and IDA, the latter by adding H_3PO_4, water, and ethanol to DGEBA before curing. The acronyms and the compositions of the prepared nanocomposites are summarized in Table 1. In a typical synthesis, 15 g of DGEBA was used and cured with 26 wt % of hardener. The DGEBA/IDA ratio was not changed in the preparation of the hybrid samples due to the low concentration of APTES and H_3PO_4 with respect to DGEBA.

4.2. Characterization. **Solid-state** ^{29}Si, ^{31}P, and ^{13}C NMR spectra were collected on a Bruker Avance II 400 spectrometer (Bruker Biospin, Milan, Italy) equipped with a 4 mm broadband magic-angle spinning (MAS) probe. Powder samples were packed in 4 mm zirconia rotors sealed with Kel-F caps and spun at 8 kHz. A ^{1}H-^{29}Si cross-polarization (CP-MAS) scheme was applied to record silicon spectra, with a ^{1}H $\pi/2$ pulse width of 3.9 μs, a contact time of 6 ms, and a recycle delay of 4 s. High-power proton decoupling was applied during the acquisition, and 20 000 scans were averaged for each spectrum. A Direct Polarization (DP) scheme with high-power proton decoupling was applied to record ^{31}P spectra with the following parameters: a $\pi/2$ pulse width of 5 μs, a recycle delay of 60 s, and 2048 scans. The recycle delay was optimized by comparing spectra acquired at different delays to ensure complete relaxation of all ^{31}P signals. ^{13}C spectra were recorded in cross-polarization mode, with a ^{1}H $\pi/2$ pulse width of 3.9 μs, a contact time of 2 ms, and a recycle delay of 4 s, applying high-power proton decoupling during the acquisition and averaging 10000 scans. Spectra deconvolution was carried out using Gaussian lines by means of the Thermo Scientific GRAMS/AI software suite.

A Nicolet 5700 **Fourier-transform infrared** (FTIR) spectrometer (Thermo Fisher, Waltham, MA), coupled with a single-reflection **attenuated total reflectance** (ATR) accessory, was used to collect ATR-IR spectra of all of the prepared samples to verify the completeness of the curing process and the consistency of the chemical composition. All of the spectra were recorded with a resolution of 4 cm^{-1} and 32 scans and the Thermo Scientific OMNIC Software Suite (v7.2, Thermo Fisher, Waltham, MA, 2005). The spectra were normalized on some specific bands, mainly 1607 and 1509 cm^{-1}, linked to the C═C bonds of the benzene rings present in the epoxy resin structure, which are not affected by the curing reactions.

High-resolution transmission electron microscopy (HRTEM) images of modified epoxy resin with phosphorus and hybrid nanocomposites were collected by using a TEM/STEM JEOL JEM 2200 fs microscope working at 200 kV. Before performing the TEM observation, the analyzed samples were powdered and dispersed in water, then a drop of the dispersed sample was laid on a Lacey Carbon film copper TEM grid, which was subsequently dried overnight in an oven at 40 °C. A population of 90 particles was selected randomly and analyzed by Image J software to estimate the particle size and distribution. Image J software was also used to determine the lattice plane distance from the HRTEM images.

To measure the storage (E') and the loss moduli versus temperature, **dynamic mechanical analysis** (DMA) was performed with a Q800 TA Instrument (New Castle) in the single-cantilever configuration on rectangular specimens (size: 35 × 10 × 4 mm^3). A ramp-up of temperature from −30 to 150 °C, at 2 °C/min and 1 Hz of frequency, was used to characterize the systems. The glass transition temperature (Tg) of the prepared systems was measured as the temperature at which the maximum damping occurs ($\tan \delta_{max}$).

The morphology characteristic of the residual char after cone calorimeter tests of pristine resin, modified resin with phosphorus and hybrid epoxy nanocomposite (EPO_2Si1P) was investigated by means of EVO 15 **scanning electron microscope** (SEM) from Zeiss (Oberkochen, Germany). The microscope was coupled to an Ultim Max 40 **energy-dispersive X-ray** (EDX) micro-analyzer, integrated with AZtecLive software, by Oxford Instruments (High Wycombe, U.K.).

A NETZSCH TG 209 F1 instrument (NETZSCH-Gerätebau GmbH, Selb, Germany) was exploited to carry out **thermogravimetric (TG) analyses** on all of the prepared samples both in nitrogen and air atmospheres (gas flow: 50 mL/min). The analyses were performed from 25 to 800 °C at a ramp of 10 °C/min.

A DSC 214 Polyma instrument (NETZSCH-Gerätebau GmbH, Selb, Germany) working under a N_2 flow (50 mL/min) was used to perform **differential scanning calorimetry** (DSC) measurements according to the following cycle: 1st heating up from 20 to 300 °C at 10 °C/min, cooling down from 300 to 20 °C at −10 °C/min, 2nd heating up from 20 to 300 °C at 10 °C/min.

The **cone calorimetry tests** were performed with a cone calorimeter (Noselab ATS, Monza, Italy) operating with an irradiative heat flux of 35 kW/m^2 (ISO 5660 standard) on specimens (100 × 100 × 3 mm^3) laid horizontally without any grid. The peak of the heat release rate (pkHRR), heat release rate (HRR), total smoke release (TSR), average specific extinction area (SEA), and total heat release (THR) were measured.

Pyrolysis combustion flow calorimetry (PCFC) tests were carried out on a Fire Testing Technology apparatus (London, UK) and according to the ASTM D7309 standard. More in detail, in the pyrolysis zone, ∼7 mg of sample were heated from 150 to 750 °C at a heating rate of 1.0 °C/s.

UL94 vertical flame spread tests were performed to assess the flammability of all epoxy-based composite by following IEC 60695-11-10 on 13 × 125 × 3 mm^3 samples.

Limiting oxygen index (LOI) tests were carried out by means of a FIRE oxygen index apparatus according to the ASTM D2863 standard.

■ ASSOCIATED CONTENT

Supporting Information

The Supporting Information is available free of charge at https://pubs.acs.org/doi/10.1021/acsanm.3c00590.

^{29}Si, ^{31}P, and ^{13}C solid-state NMR spectra of blank samples and Si/P hybrid epoxy nanocomposites; ATR-FTIR spectra of blank samples and Si/P hybrid epoxy nanocomposites; HRTEM images of the blank sample and Si/P hybrid epoxy nanocomposites; the distribution of sizes of lamellar crystalline nanodomains; DSC curves of blank samples and Si/P hybrid epoxy nanocomposites; storage modulus vs temperature from DMA data of blank samples and Si/P hybrid epoxy nanocomposites; and thermal data obtained from PCFC and cone calorimeter tests of the blank samples and Si/P hybrid epoxy nanocomposites (PDF)

https://doi.org/10.1021/acsanm.3c00590
ACS Appl. Nano Mater. 2023, 6, 7422−7435

AUTHOR INFORMATION

Corresponding Authors

Aurelio Bifulco − *Department of Chemical Materials and Production Engineering (DICMaPI), University of Naples Federico II, 80125 Naples, Italy;* orcid.org/0000-0002-4214-5385; Email: aurelio.bifulco@unina.it

Claudio Imparato − *Department of Chemical Materials and Production Engineering (DICMaPI), University of Naples Federico II, 80125 Naples, Italy;* orcid.org/0000-0003-1725-7008; Email: claudio.imparato@unina.it

Authors

Roberto Avolio − *Institute for Polymers, Composites and Biomaterials, National Research Council of Italy, 80078 Pozzuoli, Naples, Italy*

Sandro Lehner − *Laboratory for Advanced Fibers, Empa Swiss Federal Laboratories for Materials Science and Technology, 9014 St. Gallen, Switzerland*

Maria Emanuela Errico − *Institute for Polymers, Composites and Biomaterials, National Research Council of Italy, 80078 Pozzuoli, Naples, Italy*

Nigel J. Clayden − *School of Chemistry, University of East Anglia, Norwich NR4 7TJ, U.K.*

Robin Pauer − *Advanced Materials and Surfaces, Empa, Swiss Federal Laboratories for Materials Science and Technology, 8600 Dübendorf, Switzerland*

Sabyasachi Gaan − *Laboratory for Advanced Fibers, Empa Swiss Federal Laboratories for Materials Science and Technology, 9014 St. Gallen, Switzerland;* orcid.org/0000-0001-9891-5249

Giulio Malucelli − *Department of Applied Science and Technology, Politecnico di Torino, Alessandria 15121 Turin, Italy;* orcid.org/0000-0002-0459-7698

Antonio Aronne − *Department of Chemical Materials and Production Engineering (DICMaPI), University of Naples Federico II, 80125 Naples, Italy;* orcid.org/0000-0002-2711-6789

Complete contact information is available at: https://pubs.acs.org/10.1021/acsanm.3c00590

Author Contributions

This manuscript was written through contributions of all authors. All authors have given approval to the final version of the manuscript.

Notes

The authors declare no competing financial interest.

ACKNOWLEDGMENTS

The authors thank Ms. Milijana Jovic (Advanced Fibers, Empa, St. Gallen, Switzerland) for her support during the thermal and pyrolysis combustion flow calorimeter tests.

REFERENCES

(1) Oliwa, R.; Heneczkowski, M.; Oleksy, M.; Galina, H. Epoxy composites of reduced flammability. *Composites, Part B* **2016**, *95*, 1−8.

(2) Katsoulis, C.; Kandare, E.; Kandola, B. K. The combined effect of epoxy nanocomposites and phosphorus flame retardant additives on thermal and fire reaction properties of fiber-reinforced composites. *J. Fire Sci.* **2011**, *29*, 361−383.

(3) Shimizu, T.; Kanamori, K.; Nakanishi, K. Silicone-based organic−inorganic hybrid aerogels and xerogels. *Chem.−Eur. J.* **2017**, *23*, 5176−5187.

(4) Toldy, A.; Szolnoki, B.; Marosi, G. Flame retardancy of fiber-reinforced epoxy resin composites for aerospace applications. *Polym. Degrad. Stab.* **2011**, *96*, 371−376.

(5) Guadagno, L.; Raimondo, M.; Vittoria, V.; Vertuccio, L.; Naddeo, C.; Russo, S.; De Vivo, B.; Lamberti, P.; Spinelli, G.; Tucci, V. Development of epoxy mixtures for application in aeronautics and aerospace. *RSC Adv.* **2014**, *4*, 15474−15488.

(6) Mathews, L. D.; Capricho, J. C.; Peerzada, M.; Salim, N. V.; Parameswaranpillai, J.; Hameed, N. Recent Progress and Multifunctional Applications of Fire-retardant Epoxy Resins. *Mater. Today Commun.* **2022**, *33*, No. 104702.

(7) Wang, K.; Liu, H.; Wang, C.; Huang, W.; Tian, Q.; Fu, Q.; Yan, W. Flame-Retardant Performance of Epoxy Resin Composites with SiO2 Nanoparticles and Phenethyl-Bridged DOPO Derivative. *ACS Omega* **2021**, *6*, 666−674.

(8) Van der Veen, I.; de Boer, J. Phosphorus flame retardants: properties, production, environmental occurrence, toxicity and analysis. *Chemosphere* **2012**, *88*, 1119−1153.

(9) Matějka, L.; Dušek, K.; Pleštil, J.; Kříž, J.; Lednický, F. Formation and structure of the epoxy-silica hybrids. *Polymer* **1999**, *40*, 171−181.

(10) Liu, Q.; Wang, D.; Li, Z.; Li, Z.; Peng, X.; Liu, C.; Zhang, Y.; Zheng, P. Recent developments in the flame-retardant system of epoxy resin. *Materials* **2020**, *13*, 2145.

(11) Bifulco, A.; Tescione, F.; Capasso, A.; Mazzei, P.; Piccolo, A.; Durante, M.; Lavorgna, M.; Malucelli, G.; Branda, F. Effects of post cure treatment in the glass transformation range on the structure and fire behavior of in situ generated silica/epoxy hybrids. *J. Sol-Gel Sci. Technol.* **2018**, *87*, 156−169.

(12) Branda, F.; Bifulco, A.; Jehnichen, D.; Parida, D.; Pauer, R.; Passaro, J.; Gaan, S.; Pospiech, D.; Durante, M. Structure and Bottom-up Formation Mechanism of Multisheet Silica-Based Nanoparticles Formed in an Epoxy Matrix through an In Situ Process. *Langmuir* **2021**, *37*, 8886−8893.

(13) Matejka, L.; Dukh, O.; Kolařík, J. Reinforcement of crosslinked rubbery epoxies by in-situ formed silica. *Polymer* **2000**, *41*, 1449−1459.

(14) Lin, C. H.; Feng, C. C.; Hwang, T. Y. Preparation, thermal properties, morphology, and microstructure of phosphorus-containing epoxy/SiO2 and polyimide/SiO2 nanocomposites. *Eur. Polym. J.* **2007**, *43*, 725−742.

(15) Sprenger, S. Epoxy resin composites with surface-modified silicon dioxide nanoparticles: A review. *J. Appl. Polym. Sci.* **2013**, *130*, 1421−1428.

(16) Visakh, P. M.; Yoshihiko, A. *Flame Retardants: Polymer Blends, Composites and Nanocomposites*; Springer, 2015.

(17) Kashiwagi, T.; Du, F.; Douglas, J. F.; Winey, K. I.; Harris, R. H.; Shields, J. R. Nanoparticle networks reduce the flammability of polymer nanocomposites. *Nat. Mater.* **2005**, *4*, 928−933.

(18) Zhang, Y.; Yu, B.; Wang, B.; Liew, K. M.; Song, L.; Wang, C.; Hu, Y. Highly effective P−P synergy of a novel DOPO-based flame retardant for epoxy resin. *Ind. Eng. Chem. Res.* **2017**, *56*, 1245−1255.

(19) Venezia, V.; Matta, S.; Lehner, S.; Vitiello, G.; Costantini, A.; Gaan, S.; Malucelli, G.; Branda, F.; Luciani, G.; Bifulco, A. Detailed Thermal, Fire, and Mechanical Study of Silicon-Modified Epoxy Resin Containing Humic Acid and Other Additives. *ACS Appl. Polym. Mater.* **2021**, *3*, 5969−5981.

(20) Bifulco, A.; Parida, D.; Salmeia, K. A.; Nazir, R.; Lehner, S.; Stämpfli, R.; Markus, H.; Malucelli, G.; Branda, F.; Gaan, S. Fire and mechanical properties of DGEBA-based epoxy resin cured with a cycloaliphatic hardener: Combined action of silica, melamine and DOPO-derivative. *Mater. Design* **2020**, *193*, 108862.

(21) Ponyrko, S.; Kobera, L.; Brus, J.; Matějka, L. Epoxy-silica hybrids by nonaqueous sol−gel process. *Polymer* **2013**, *54*, 6271−6282.

(22) Ren, Y.; Yuan, D.; Li, W.; Cai, X. Flame retardant efficiency of KH-550 modified urea-formaldehyde resin cooperating with ammonium polyphosphate on polypropylene. *Polym. Degrad. Stab.* **2018**, *151*, 160−171.

(23) Mingfeng, C.; Huawei, Q.; Shanshan, L.; Wei, Z.; Jiashui, L.; Canpei, L.; Huagui, Z. Novel Si/N/P-Containing Flame Retardant for Epoxy Resin with Excellent Comprehensive Performance. *ChemistrySelect* **2021**, *6*, 13873−13883.
(24) Bifulco, A.; Parida, D.; Salmeia, K.; Lehner, S.; Stämpfli, R.; Markus, H.; Malucelli, G.; Branda, F.; Gaan, S. Improving Flame Retardancy of in-situ Silica-Epoxy Nanocomposites cured with Aliphatic Hardener: Combined effect of DOPO-based flame-retardant and Melamine. *Composites Part C: Open Access* **2020**, *2*, No. 100022.
(25) Chiang, C.-L.; Ma, C.-C. M. Synthesis, characterization and thermal properties of novel epoxy containing silicon and phosphorus nanocomposites by sol−gel method. *Eur. Polym. J.* **2002**, *38*, 2219−2224.
(26) Parida, D.; Salmeia, K. A.; Sadeghpour, A.; Zhao, S.; Maurya, A. K.; Assaf, K. I.; Moreau, E.; Pauer, R.; Lehner, S.; Jovic, M.; et al. Template-free synthesis of hybrid silica nanoparticle with functionalized mesostructure for efficient methylene blue removal. *Mater. Design* **2021**, *201*, No. 109494.
(27) Perret, B.; Schartel, B.; Stöß, K.; Ciesielski, M.; Diederichs, J.; Döring, M.; Krämer, J.; Altstädt, V. Novel DOPO-based flame retardants in high-performance carbon fibre epoxy composites for aviation. *Eur. Polym. J.* **2011**, *47*, 1081−1089.
(28) Agrawal, S.; Narula, A. K. Curing and thermal behaviour of a flame retardant cycloaliphatic epoxy resin based on phosphorus containing poly(amide-imide)s. *J. Therm. Anal. Calorim.* **2014**, *115*, 1693−1703.
(29) Varganici, C. D.; Rosu, L.; Lehner, S.; Hamciuc, C.; Jovic, M.; Rosu, D.; Mustata, F.; Gaan, S. Semi−interpenetrating networks based on epoxy resin and oligophosphonate: Comparative effect of three hardeners on the thermal and fire properties. *Mater. Design* **2021**, *212*, No. 110237.
(30) Aronne, A.; Turco, M.; Bagnasco, G.; Pernice, P.; Di Serio, M.; Clayden, N. J.; Marenna, E.; Fanelli, E. Synthesis of high surface area phosphosilicate glasses by a modified sol− gel method. *Chem. Mater.* **2005**, *17*, 2081−2090.
(31) Clayden, N. J.; Accardo, G.; Mazzei, P.; Piccolo, A.; Pernice, P.; Vergara, A.; Ferone, C.; Aronne, A. Phosphorus stably bonded to a silica gel matrix through niobium bridges. *J. Mater. Chem. A* **2015**, *3*, 15986−15995.
(32) Clayden, N. J.; Esposito, S.; Pernice, P.; Aronne, A. Solid state 29Si and 31P NMR study of gel derived phosphosilicate glasses. *J. Mater. Chem.* **2001**, *11*, 936−943.
(33) Sanchez, C.; Ribot, F.; Lebeau, B. Molecular design of hybrid organic-inorganic nanocomposites synthesized via sol-gel chemistry. *J. Mater. Chem.* **1999**, *9*, 35−44.
(34) Pierre, A. C. *Hybrid Organic−Inorganic and Composite Materials*; Springer, 2020; pp 421−455.
(35) Kashiwagi, T.; Gilman, J. W.; Butler, K. M.; Harris, R. H.; Shields, J. R.; Asano, A. Flame retardant mechanism of silica gel/silica. *Fire Mater.* **2000**, *24*, 277−289.
(36) Piscitelli, F.; Lavorgna, M.; Buonocore, G. G.; Verdolotti, L.; Galy, J.; Mascia, L. Plasticizing and Reinforcing Features of Siloxane Domains in Amine-Cured Epoxy/Silica Hybrids. *Macromol. Mater. Eng.* **2013**, *298*, 896−909.
(37) Piscitelli, F.; Buonocore, G. G.; Lavorgna, M.; Verdolotti, L.; Pricl, S.; Gentile, G.; Mascia, L. Peculiarities in the structure–Properties relationship of epoxy-silica hybrids with highly organic siloxane domains. *Polymer* **2015**, *63*, 222−229.
(38) Jiao, J.; Liu, P.; Wang, L.; Cai, Y. One-step synthesis of improved silica/epoxy nanocomposites with inorganic-organic hybrid network. *J. Polym. Res.* **2013**, *20*, 2145.
(39) Bifulco, A.; Imparato, C.; Aronne, A.; Malucelli, G. Flame retarded polymer systems based on the sol-gel approach: recent advances and future perspectives. *J. Sol-Gel Sci. Technol.* **2022**, 1−25.
(40) Protsak, I. S.; Morozov, Y. M.; Dong, W.; Le, Z.; Zhang, D.; Henderson, I. M. A 29Si, 1H, and 13C solid-state NMR study on the surface species of various depolymerized organosiloxanes at silica surface. *Nanoscale Res. Lett.* **2019**, *14*, 160.
(41) Jiao, C.; Zhuo, J.; Chen, X.; Li, S.; Wang, H. Flame retardant epoxy resin based on bisphenol A epoxy resin modified by phosphoric acid. *J. Therm. Anal. Calorim.* **2013**, *114*, 253−259.
(42) Corbridge, D. E. C. The structural chemistry of phosphates. *Bull. Soc. Fr. Mineral. Cristallogr.* **1971**, *94*, 271−299.
(43) Lu, L.; Qian, X.; Zeng, Z.; Yang, S.; Shao, G.; Wang, H.; Jin, J.; Xu, X. Novel phosphorus-based flame retardants containing 4-tert-butylcalix[4]arene: Preparation and application for the fire safety of epoxy resins. *J. Appl. Polym. Sci.* **2017**, *134*, 45105.
(44) García, A.; Colilla, M.; Izquierdo-Barba, I.; Vallet-Regi, M. Incorporation of phosphorus into mesostructured silicas: a novel approach to reduce the SiO2 leaching in water. *Chem. Mater.* **2009**, *21*, 4135−4145.
(45) Salmeia, K. A.; Neels, A.; Parida, D.; Lehner, S.; Rentsch, D.; Gaan, S. Insight into the synthesis and characterization of organo-phosphorus-based bridged triazine compounds. *Molecules* **2019**, *24*, 2672.
(46) D'Apuzzo, M.; Aronne, A.; Esposito, S.; Pernice, P. Sol-gel synthesis of humidity-sensitive P2O5-SiO2 amorphous films. *J. Sol-Gel Sci. Technol.* **2000**, *17*, 247−254.
(47) Sanchez, C.; Ribot, F.; Rozes, L.; Alonso, B. Design of Hybrid organic-inorganic nanocomposites synthesized via sol-gel chemistry. *Mol. Cryst. Liq. Cryst. Sci. Technol.: Section A* **2000**, *354*, 143−158.
(48) Sanchez, C.; Galo, J.; Ribot, F.; Grosso, D. Design of functional nano-structured materials through the use of controlled hybrid organic−inorganic interfaces. *C. R. Chim.* **2003**, *6*, 1131−1151.
(49) Xu, A.-W.; Yu, J. C.; Cai, Y.-P.; Zhang, H.-X.; Zhang, L.-Z. The preparation of a highly ordered long-range lamellar silica structure with large interlayer spacings. *Chem. Commun.* **2002**, *15*, 1614−1615.
(50) Toussaint, G.; Rodriguez, M. A.; Cloots, R.; Rubio, J.; Rubio, F.; Vertruyen, B.; Henrist, C. Characterization of surface and porous properties of synthetic hybrid lamellar silica. *J. Non-Cryst. Solids* **2011**, *357*, 951−957.
(51) Henrist, C.; Rulmont, A.; Cloots, R. Synthesis and characterization of inorganic, lamellar nanofillers with high aspect ratio. *J. Eur. Ceram. Soc.* **2007**, *27*, 1023−1027.
(52) Clayden, N. J.; Imparato, C.; Avolio, R.; Ferraro, G.; Errico, M. E.; Vergara, A.; Busca, G.; Gervasini, A.; Aronne, A.; Silvestri, B. Chloride-free hydrolytic sol-gel synthesis of Nb-P-Si oxides: An approach to solid acid materials. *Green Chem.* **2020**, *22*, 7140−7151.
(53) Branda, F.; Parida, D.; Pauer, R.; Durante, M.; Gaan, S.; Malucelli, G.; Bifulco, A. Effect of the Coupling Agent (3-Aminopropyl) Triethoxysilane on the Structure and Fire Behavior of Solvent-Free One-Pot Synthesized Silica-Epoxy Nanocomposites. *Polymers* **2022**, *14*, 3853.
(54) Panwar, V.; Pal, K. Dynamic Mechanical Analysis of Clay−polymer Nanocomposites. In *Clay-polymer Nanocomposites*; Elsevier, 2017; pp 413−441.
(55) Mascia, L.; Prezzi, L.; Lavorgna, M. Peculiarities in the solvent absorption characteristics of epoxy-siloxane hybrids. *Polym. Eng. Sci.* **2005**, *45*, 1039−1048.
(56) Lange, R. F. M.; Meijer, E. W. Supramolecular polymer interactions based on the alternating copolymer of styrene and Maleimide. *Macromolecules* **1995**, *28*, 782−783.
(57) Wang, F.; Pan, S.; Zhang, P.; Fan, H.; Chen, Y.; Yan, J. Synthesis and application of phosphorus-containing flame retardant plasticizer for polyvinyl chloride. *Fibers Polym.* **2018**, *19*, 1057−1063.
(58) Aouf, C.; Nouailhas, H.; Fache, M.; Caillol, S.; Boutevin, B.; Fulcrand, H. Multi-functionalization of gallic acid. Synthesis of a novel bio-based epoxy resin. *Eur. Polym. J.* **2013**, *49*, 1185−1195.
(59) Savonnet, E.; Grau, E.; Grelier, S.; Defoort, B.; Cramail, H. Divanillin-based epoxy precursors as DGEBA substitutes for biobased epoxy thermosets. *ACS Sustainable Chem. Eng.* **2018**, *6*, 11008−11017.
(60) Zabihi, O.; Aghaie, M.; Zare, K. Study on a novel thermoset nanocomposite form DGEBA−cycloaliphatic diamine and metal nanoparticles: thermal properties and curing behavior. *J. Therm. Anal. Calorim.* **2013**, *111*, 703−710.

https://doi.org/10.1021/acsanm.3c00590
ACS Appl. Nano Mater. 2023, 6, 7422−7435

(61) Zhu, Z.-M.; Wang, L.-X.; Lin, X.-B.; Dong, L.-P. Synthesis of a novel phosphorus-nitrogen flame retardant and its application in epoxy resin. *Polym. Degrad. Stab.* **2019**, *169*, No. 108981.
(62) Salmeia, K. A.; Gooneie, A.; Simonetti, P.; Nazir, R.; Kaiser, J.-P.; Rippl, A.; Hirsch, C.; Lehner, S.; Rupper, P.; Hufenus, R.; Gaan, S. Comprehensive study on flame retardant polyesters from phosphorus additives. *Polym. Degrad. Stab.* **2018**, *155*, 22−34.
(63) Gilman, J. W.; Harris, R. H., Jr; Shields, J. R.; Kashiwagi, T.; Morgan, A. B. A study of the flammability reduction mechanism of polystyrene-layered silicate nanocomposite: layered silicate reinforced carbonaceous char. *Polym. Adv. Technol.* **2006**, *17*, 263−271.
(64) Jian, R.; Wang, P.; Duan, W.; Wang, J.; Zheng, X.; Weng, J. Synthesis of a novel P/N/S-containing flame retardant and its application in epoxy resin: thermal property, flame retardance, and pyrolysis behavior. *Ind. Eng. Chem. Res.* **2016**, *55*, 11520−11527.
(65) Lyon, R. E.; Walters, R. N. Pyrolysis combustion flow calorimetry. *J. Anal. Appl. Pyrolysis* **2004**, *71*, 27−46.
(66) Li, A.; Mao, P.; Liang, B. The application of a phosphorus nitrogen flame retardant curing agent in epoxy resin. *e-Polymers* **2019**, *19*, 545−554.
(67) Zhang, W.; Fina, A.; Ferraro, G.; Yang, R. FTIR and GCMS analysis of epoxy resin decomposition products feeding the flame during UL 94 standard flammability test. Application to the understanding of the blowing-out effect in epoxy/polyhedral silsesquioxane formulations. *J. Anal. Appl. Pyrolysis* **2018**, *135*, 271−280.
(68) Schartel, B. Phosphorus-based flame retardancy mechanisms—old hat or a starting point for future development? *Materials* **2010**, *3*, 4710−4745.
(69) Liu, L.; Xu, Y.; Xu, M.; Li, Z.; Hu, Y.; Li, B. Economical and facile synthesis of a highly efficient flame retardant for simultaneous improvement of fire retardancy, smoke suppression and moisture resistance of epoxy resins. *Composites, Part B* **2019**, *167*, 422−433.
(70) Bifulco, A.; Marotta, A.; Passaro, J.; Costantini, A.; Cerruti, P.; Gentile, G.; Ambrogi, V.; Malucelli, G.; Branda, F. Thermal and fire behavior of a bio-based epoxy/silica hybrid cured with methyl nadic anhydride. *Polymers* **2020**, *12*, 1661.

https://doi.org/10.1021/acsanm.3c00590
ACS Appl. Nano Mater. 2023, 6, 7422−7435